

## An Evaluation of MÉRA, a High-Resolution Mesoscale Regional Reanalysis

EOIN WHELAN, EMILY GLEESON, AND JOHN HANLEY

*Met Éireann, Dublin, Ireland*

(Manuscript received 18 December 2017, in final form 11 July 2018)

### ABSTRACT

Met Éireann, the Irish Meteorological Service, has generated a very high resolution (2.5-km horizontal grid) regional climate reanalysis for Ireland called the Met Éireann Reanalysis (MÉRA). MÉRA spans the period from 1981 to 2015 and was produced using the shared ALADIN–HIRLAM numerical weather prediction system. This article includes comparisons with the ERA-Interim and Uncertainties in Ensembles of Regional Reanalyses (UERRA) datasets, analysis of data assimilation outputs, precipitation comparisons, and a focus on extremes of wind and rainfall. The comparisons with the reanalysis datasets show that MÉRA provides a high-quality reconstruction of recent Irish climate and benefits from the use of a very high resolution grid, in particular in relation to wind and precipitation extremes.


### 1. Introduction

Climate reanalysis is a well-established approach for recreating past climate, monitoring climate in real time, and for the validation and calibration of numerical weather prediction (NWP) models. Reanalysis datasets have uses outside of meteorology and climatology as they are generated using a fixed version of an NWP model that utilizes historical observations and they produce parameters that are physically consistent and often not routinely observed. Thus, climate reanalyses have the potential to extend the knowledge gained from current observation networks.

The concept of atmospheric reanalysis originated with the production of datasets by ECMWF and GFDL (acronyms not expanded in this paper can be found at <https://www.ametsoc.org/pubsacronymlist>) for the 1979 Global Weather Experiment (Fleming et al. 1979). Since then, the production of global reanalysis datasets has become a well-established activity. Examples of such datasets include the ECMWF Reanalysis (ERA) series [ERA-15 (Gibson et al. 1997), ERA-40 (Uppala et al. 2005), ERA-Interim (Dee et al. 2011), and ERA-5 (Hersbach and Dee 2016)], JMA's Japanese Reanalysis (JRA) series [JRA-25 (Onogi et al. 2007) and JRA-55

(Kobayashi et al. 2015)] and NASA's Modern-Era Retrospective Analysis for Research and Applications (MERRA) series [MERRA (Rienecker et al. 2011) and MERRA-2 (Gelaro et al. 2017)]. The production of new reanalysis datasets has benefited from advances in data assimilation techniques, better use of observations, improved forecast models, and higher-resolution model configurations. The coupling of atmosphere–land–ocean systems or Earth system models (e.g., ECMWF's ERA-20C and ERA-20CM; Hersbach et al. 2013; Poli et al. 2013) and improved use of atmospheric composition information, such as CMIP5 (Taylor et al. 2012) data, have enhanced the quality of reanalysis datasets. More recently, reanalysis uncertainty has been estimated using ensemble techniques, for example in ERA-5 (Hersbach and Dee 2016).

Because of computational constraints, global reanalyses cannot be run at the very high resolutions required to resolve mesoscale processes. However, high-resolution regional reanalyses can be produced using limited-area NWP models (LAMs). LAMs can be run at higher temporal and spatial resolutions so that focus can be put on near-surface parameters, weather extremes, and frequency distributions of weather parameters. In particular, the analysis of extremes provides a rigorous test of the performance of reanalysis datasets and the utilization of reanalyses in this area is extremely useful for planning and emergency management. High-resolution regional reanalyses have already been produced for Europe, Asia, and North America. Examples

 Denotes content that is immediately available upon publication as open access.

*Corresponding author:* Eoin Whelan, [eoin.whelan@met.ie](mailto:eoin.whelan@met.ie)

DOI: 10.1175/JAMC-D-17-0354.1

© 2018 American Meteorological Society. For information regarding reuse of this content and general copyright information, consult the [AMS Copyright Policy](#) ([www.ametsoc.org/PUBSReuseLicenses](http://www.ametsoc.org/PUBSReuseLicenses)).

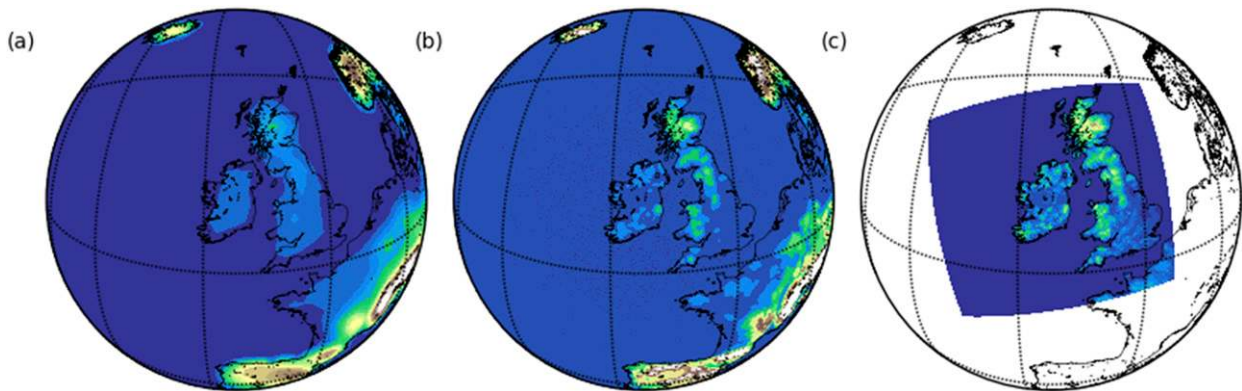


FIG. 1. (a) ERA-Interim (79-km grid spacing), (b) UERRA HARMONIE-ALADIN (11-km grid spacing), and (c) MÉRA (2.5-km grid spacing) orographies.

include a regional reanalysis covering the European continent at 6-km horizontal resolution (COSMO-REA6; Kaiser-Weiss et al. 2015; Bollmeyer et al. 2015), the High Resolution Limited Area Model (HIRLAM) reanalysis (Dahlgren et al. 2016), the Indian Monsoon Data Assimilation and Analysis regional reanalysis project (Mahmood et al. 2018), and the North American Regional Reanalysis (Mesinger et al. 2006). The Arctic System Reanalysis (ASR) series [ASRv1 (Bromwich et al. 2010) and ASRv2 (Bromwich et al. 2010)] has produced reanalyses of the Arctic climate. Of late, more localized regional reanalyses have been produced for the Baltic Sea (Luhamaa et al. 2011), the Netherlands (Steppek et al. 2015), and Iceland (Nawri 2014), with recent European projects, such as European Reanalysis and Observations for Monitoring (EURO4M; Klein Tank 2010) and Uncertainties in Ensembles of Regional Reanalyses (UERRA; European Commission 2017), combining results from several European regional reanalyses to include estimations of uncertainties.

Despite the availability of reanalysis datasets for Europe, no very high resolution (mesoscale) reanalysis dataset had been produced for Ireland. We have run the HIRLAM-ALADIN Research on Mesoscale Operational NWP in Euromed (HARMONIE-AROME) canonical configuration of the shared ALADIN-HIRLAM NWP system, hereinafter HARMONIE-AROME, on a 2.5-km horizontal grid for the 35-yr period 1981–2015 with the aim of improving our knowledge of Ireland's climate and its weather extremes. This reanalysis dataset, called the Met Éireann Reanalysis (MÉRA), was produced using the same domain as has been used operationally by Met Éireann from 2011 to 2018. The domain covers Ireland, the United Kingdom, and an area of northern France (Fig. 1c). The extra orographic information gained by using the 2.5-km grid can be

appreciated when compared with the (global) ERA-Interim (~79 km; Fig. 1a) and UERRA HARMONIE-ALADIN (~11 km; Fig. 1b) grids. The MÉRA project was completed in early 2017, and the dataset was published in May 2017.

This paper is a successor to an earlier paper (Gleeson et al. 2017), which summarized the progress of the project, and provides a more complete evaluation of the dataset, including a study of how well the dataset captures extremes of wind and precipitation. It is laid out as follows. Section 2 provides details on the model configuration and MÉRA simulations carried out. Section 3 describes the inputs used by the model. The performances of the data assimilation system and forecast model are evaluated in sections 4 and 5. This paper finishes with discussions and conclusions in section 6.

## 2. Model description

The following model description parallels that of Gleeson et al. (2017) but is outlined in greater detail and included here for completeness. The application of the NWP system used to produce the MÉRA dataset is summarized in the process diagram in Fig. 2 and is described in more detail below.

### a. The forecast model

The shared ALADIN-HIRLAM NWP system is used for operational weather forecasting by 26 national meteorological services in Europe and North Africa that form the HIRLAM and ALADIN consortia. Pottier (2016) summarizes 42 limited area configurations of the system used by the consortia members and a history of the collaboration between the ALADIN and HIRLAM partners is provided in the introduction of Bengtsson

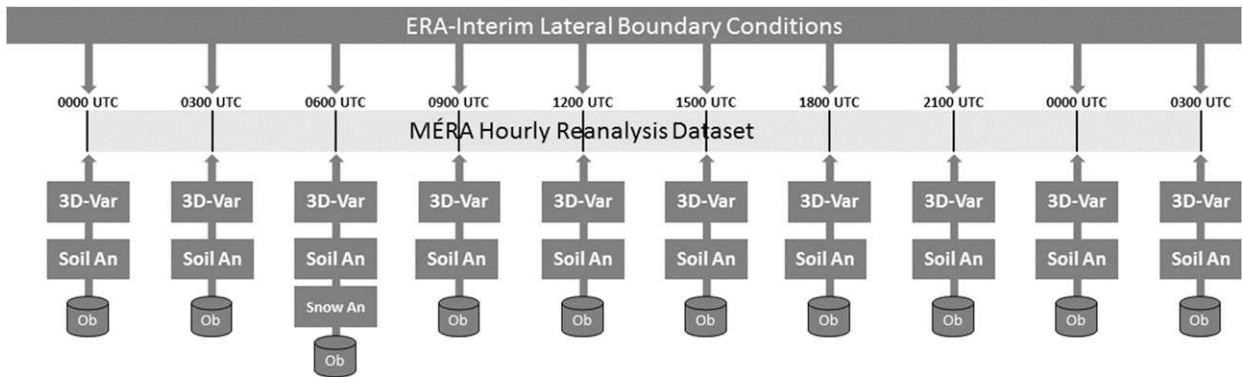


FIG. 2. Process diagram of the MÉRA system.

et al. (2017). The HARMONIE–AROME canonical configuration of version 38h1.2 of this system, based on Seity et al. (2011), was used for the MÉRA project. The MÉRA setup uses a  $540 \times 500$  horizontal grid on a Lambert conformal projection with 2.5-km spacing at the center and 65 vertical levels. The lowest level is at 12 m, with a nominal model top at 10 hPa and an integration time step of 60 s. ALADIN nonhydrostatic dynamics (Bénard et al. 2010), nonhydrostatic mesoscale (Meso-NH) physics (Lafore et al. 1998), and the Surface Externalisée (SURFEX) externalized surface scheme (Masson et al. 2013) are used. Further details on the dynamical core and physics and surface parameterizations are provided.

HARMONIE–AROME is a mesoscale, spectral, nonhydrostatic model with a dynamical core developed by the ALADIN consortium (Bubnová et al. 1995; Bénard et al. 2010). It is based on the fully compressible Euler equations. The evolution of the equations is discretized in time and space using a two-time-level, semi-implicit, semi-Lagrangian (SL) discretization scheme on an A grid and a mass-based hybrid pressure terrain-following coordinate (Simmons and Burridge 1981; Laprise 1992). Most prognostic variables have a spectral representation based on a double Fourier decomposition and a vertical discretization based on finite differences (Simmons and Burridge 1981). Horizontal diffusion is applied both by linear spectral diffusion and nonlinear flow-dependent diffusion, which acts through SL advection and, thus, was given the name semi-Lagrangian horizontal diffusion (Vána et al. 2008; Bengtsson et al. 2012).

A more in-depth discussion of the physics and surface parameterizations can be found in Seity et al. (2011), Masson et al. (2013), Bengtsson et al. (2017), and Termonia et al. (2017). Shortwave and longwave radiation, clouds and cloud microphysics, turbulence, and shallow convection are parameterized in the model.

Using a 2.5-km grid spacing, deep convection is expected to be approximately resolved and explicitly represented by the model’s nonhydrostatic dynamics. There is, thus, no parameterization of deep convection. The schemes used in HARMONIE–AROME are described below and summarized in Table 1.

The default shortwave (SW) radiation parameterization is the Morcrette scheme from ECMWF’s Integrated Forecasting System (IFS) cycle 25R1 containing six spectral intervals. The default longwave (LW) radiation scheme contains 16 spectral bands and uses the Rapid Radiative Transfer Model of Mlawer et al. (1997). Both the SW and LW schemes are described in Morcrette (1991) and ECMWF (2003). The microphysics scheme used in AROME-France and HARMONIE–AROME is a one-moment bulk scheme, which uses a three-class ice parameterization, referred to as ICE3, originally developed for Meso-NH (Pinty and Jabouille 1998; Lascaux et al. 2006). The scheme used to compute sedimentation is described in Bouteloup et al. (2011). The Cuxart–Bougeault–Redelsperger (CBR) scheme (Cuxart et al. 2000; Seity et al. 2011) is used to parameterize subgrid turbulence. This scheme is based on a prognostic turbulent kinetic energy equation with a diagnostic mixing length as described in Bougeault and Lacarrère (1989). Shallow convection is parameterized using the eddy-diffusivity mass-flux (EDMFm) framework (de Rooy and Siebesma 2008). The differences between EDMFm and the eddy diffusivity Kain–Fritsch (EDKF) scheme that is the default in AROME-France are described in Bengtsson et al. (2017).

Surface processes in HARMONIE–AROME are handled by the SURFEX (version 7.2) externalized surface scheme (Masson et al. 2013). SURFEX is a modeling platform, mainly developed by Météo-France in collaboration with the scientific community, and comprises a set of physical models for natural land surfaces, urban areas, lakes, and oceans.

TABLE 1. Physics parameterizations used by MÉRA.

Parameterization	Scheme	Reference
Radiation	LW16, SW6	Morcrette (1991); ECMWF (2003)
Turbulence	CBR	Cuxart et al. (2000); Bougeault and Lacarrère (1989)
Microphysics	ICE3	Pinty and Jabouille (1998)
Sedimentation	—	Bouteloup et al. (2011)
Shallow convection	EDMFm	de Rooy and Siebesma (2008)
Deep convection	—	

Exchanges of energy between the land surface and the atmosphere in the nature tile are modeled by the Interactions between Soil, Biosphere, and Atmosphere (ISBA) scheme with a three-level force–restore approach (Boone et al. 1999). Tiles representing natural land surfaces are subdivided into patches depending on the vegetation type. However, only one patch is used in the version in MÉRA, which means that the energy budgets for all of the vegetation types present in ISBA are aggregated. The Exchange Coefficients from Unified Multicampaign Estimates (ECUME) scheme by Belamari (2005) is used over water for the sea tile. The inland water tile, which comprises rivers and lakes, is described by the Charnock (1955) formula. The fourth tile, urban regions, is simulated using the Town Energy Balance (TEB) model (Masson 2000)

### b. Data assimilation

Data assimilation is used to calculate the initial state of the surface and atmosphere for an NWP (forecast) model using observations in addition to a priori model-state information, called the background. The MÉRA reanalysis uses a 3-h cycle to progress the model state forward in time. Every three hours, observations are combined with information from the previous 3-h forecast to produce an estimate of the state of the surface and atmosphere. Optimal interpolation (OI) techniques are used to produce the surface analysis, and three-dimensional variational data assimilation (3D-Var) is used to produce the upper-air analysis for each cycle. An analysis window of 3 h centered on the analysis time is used by 3D-Var, with observations reported within this time window being assimilated. Only observations at the analysis time are assimilated by the surface OI assimilation scheme. The observations assimilated by MÉRA are described in further detail in section 3a.

The OI assimilation scheme used to update MÉRA surface and soil parameters is described in Giard and Bazile (2000) and implemented in the SURFEX model (Masson et al. 2013). Soil temperature and moisture values are updated using screen-level observations of temperature and humidity from “SYNOP” reports. Following Giard and Bazile (2000), the soil analysis formulation can be generalized as

$$\Delta X_i = \alpha_i^T \Delta T_{2m} + \alpha_i^H \Delta H_{2m},$$

where  $X_i$  are the soil analysis variables (temperature  $T$  and moisture  $H$ ) for the surface (subscript  $s$ ) and an average soil value (subscript  $p$ ),  $\Delta$  is the analysis increment, and  $\alpha_{s/p}^{T/H}$  are the OI coefficients. The  $\alpha_i^{T/H}$  for soil temperature are constant, and the  $\alpha_i^{T/H}$  for soil moisture depend on the diurnal cycle and vegetation fraction. More detail on the formulation of the OI coefficients can be found in Giard and Bazile (2000) and Mahfouf et al. (2009). An OI snow analysis is carried out once per day at 0600 UTC using observations of snow depth from SYNOP reports. The OI scheme does not perform an analysis of the sea surface temperature (SST) or sea ice concentration (SIC). Instead, ERA-Interim SST and SIC values are interpolated to the MÉRA grid and used directly by the model.

The atmospheric state is updated using HARMONIE–AROME’s implementation of 3D-Var, as described in Fischer et al. (2005), which benefits from the original incremental implementation of 3D-Var in ECMWF’s IFS (Courtier et al. 1998). The incremental formulation minimizes the cost function  $J$ :

$$J(\delta \mathbf{x}) = 0.5 \delta \mathbf{x}^T \mathbf{B}^{-1} \delta \mathbf{x} + 0.5 (\mathbf{H} \delta \mathbf{x} - \mathbf{d})^T \mathbf{R}^{-1} (\mathbf{H} \delta \mathbf{x} - \mathbf{d}),$$

where  $\mathbf{x}$  is the model state vector,  $\delta \mathbf{x}$  is the model-state increment, and, at the cost function minimum, the analysis increment  $\delta \mathbf{x}^a$  is added to the background  $\mathbf{x}^b$ . Here,  $\mathbf{B}$  and  $\mathbf{R}$  are the background error and observation error covariance matrices, respectively;  $\mathbf{H}$  is a linear approximation of the observation operator  $H$  (not the same as the moisture variable above), and  $\mathbf{d}$ , the innovation vector, is defined as

$$\mathbf{d} = \mathbf{y} - \mathbf{H} \mathbf{x}^b,$$

where  $\mathbf{y}$  is the observation vector. The derivation of the background error covariance matrix,  $\mathbf{B}$  is described in Brousseau et al. (2011). The error statistics used by the MÉRA 3D-Var assimilation system are based on differences between 6-h forecasts from a four-member ensemble of downscaled IFS ensemble forecasts run for 40 cycles. As noted in Gleeson et al. (2017), deriving

TABLE 2. Summary of output available on pressure, height, and surface levels.

Level type	Parameter	Level
Pressure	Temperature, wind, cloud, relative humidity, and geopotential	100, 200, 300, 400, 500, 600, 700, 800, 850, 900, 925, 950, and 1000 hPa
Height above ground	Temperature, wind, and relative humidity	30, 50, 60, 70, 80, 90, 100, 125, 150, 200, 300, and 400 m
Soil	Temperature, moisture, and ice	0, 20, and 300 cm (below the surface)
Surface	Precipitation diagnostics	Surface
Diagnostic	Screen-level parameters	2 and 10 m for winds and gusts
Surface	Radiative and nonradiative fluxes	Surface
Top of atmosphere	Radiative and nonradiative fluxes	Nominal top of atmosphere

the structure functions would benefit from using forecast data that span the diurnal cycle and are from different seasons. Also, longer forecast integrations may be required to produce more realistic convective-scale spectra, as noted in [Arriola et al. \(2016\)](#).

Observations within 100 km of the lateral boundaries are excluded from the data assimilation system. This is to prevent the wraparound of spurious analysis increments due to the biperiodic formulation of the model and the use of a narrow (11 grid point) extension zone ([Lindskog et al. 2010](#)). Aircraft data are thinned to about 25 km to avoid violating the assumption of independent observations errors made in the 3D-Var formulation. The observation error statistics used by 3D-Var are defined for each observation type at standard pressure levels and interpolated to the observation heights in the observations preprocessing step. These values have been estimated by statistically evaluating the performance of observations in operational data assimilation systems over long periods of time using methods, as described in [Desroziers et al. \(2005\)](#).

Large-scale information from the ERA-Interim lateral boundary conditions (LBC) are used to adjust the background information before the 3D-Var step, as described in [Dahlgren \(2013\)](#). This method of blending larger scales from the nesting model is used instead of adding an extra term  $J_k$  to the cost function ([Guidard and Fischer 2008](#)).

### c. Production and output

This description of the reanalysis dataset production parallels that of [Gleeson et al. \(2017\)](#). Seven parallel simulations were set up to run for 6 yr at a time with a 1-yr spinup period for each simulation. Therefore, each spinup year (1985, 1990, 1995, 2000, 2005, 2010) overlaps with corresponding production year; the overlapping years were used to evaluate the spinup process of subsoil parameters. A spinup period of 1 yr was deemed necessary to allow deep soil parameters to reach an equilibrium (see [Gleeson et al. 2017](#)).

Three-hourly analysis output is available. Forecast model output is available for each forecast hour up to

33 h for the 0000 UTC forecast and to 3 h otherwise. A small subset of the surface output is available at analysis times and for each 3-h forecast while upper-air data are available on pressure levels and a selection of near-surface levels. The analysis and forecast output data are summarized in [Table 2](#) and described more comprehensively in [Whelan et al. \(2017\)](#). MÉRA data are freely available under the Creative Commons Attribution 4.0 International (CC BY 4.0) license. Access to the dataset can be arranged with the authors.

## 3. Reanalysis inputs

### a. Observations used

Conventional observations available in ECMWF's Meteorological Archival and Retrieval System (MARS archive) were assimilated by MÉRA's surface OI and upper-air 3D-Var schemes. The reanalysis production would have benefited from the assimilation of satellite observations (radiances and scatterometer winds) and radar observations (reflectivities), and HARMONIE-AROME is capable of processing and assimilating these observations. However, it was decided prior to production that the gathering, preparation, testing, and monitoring of such observations was beyond the resources of this project.

From 1981 to 2004 observations stored in the operational data assimilation stream were used, between July 2004 and November 2013 observations stored in the delayed cutoff data assimilation stream were used, and after November 2013 observations stored in the long-window data assimilation stream were used. These data sources were selected to reuse the conventional observations assimilated by the ERA-Interim project.

Observations of temperature at 2 m ( $T_{2m}$ ) and relative humidity at 2 m ( $RH_{2m}$ ) from SYNOP reports were assimilated every 3 h by the OI surface data assimilation scheme with SYNOP snow-depth observations assimilated once per day, as described earlier in [section 2b](#). A time series of the OI observation usage for the reanalysis period is shown in [Fig. 3a](#). There is an increase in the

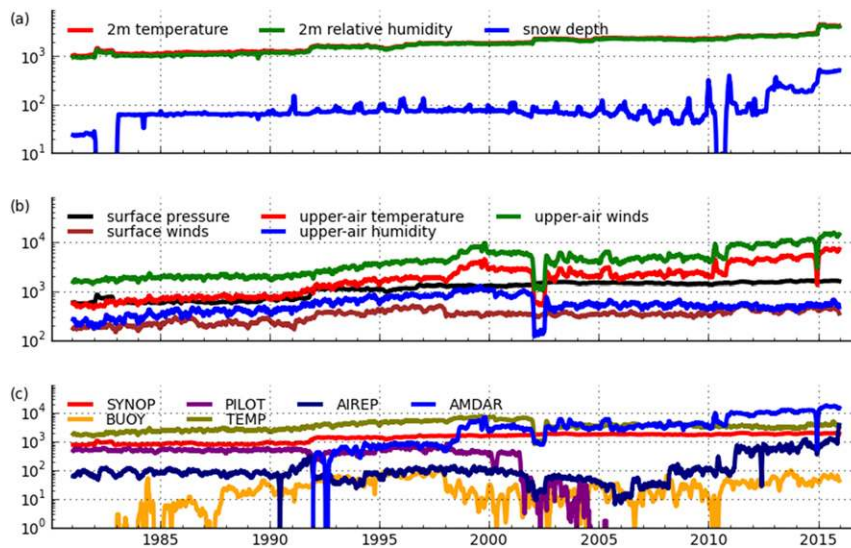


FIG. 3. Daily counts of (a) of screen-level observations used by the OI surface data assimilation system, (b) observations assimilated by MÉRA's 3D-Var, and (c) observations classified by report type assimilated in MÉRA. A 30-day running average is applied to all observation time series data.

number of SYNOP reports assimilated by MÉRA throughout the reanalysis period increasing from about 1000 observations per day in 1981 to about 4000 per day in 2015. The seasonal variation in availability of SYNOP snow observations can be seen also.

Observations of surface pressure (SYNOP, "SHIP," and "BUOY"), surface winds (SYNOP and SHIP over sea), upper-air temperatures ("TEMP," "AIREP," and "AMDAR"), winds (TEMP, "PILOT," AIREP, and AMDAR), and humidity (TEMP) were assimilated every 3 h. Aircraft Communications Addressing and Reporting System (ACARS) aircraft reports were not used because of a bug in the observation preprocessing step of the data assimilation system. Figure 3b shows the number of observations assimilated by MÉRA's 3D-Var classified by observation variable, and Fig. 3c shows the observation numbers classified by observation type. As reported by Dahlgren et al. (2016), there is a drop in the number of upper-air data stored in the MARS archive during 2002 and a brief dip in AIREP observation numbers at the end of 2014. There is an increase in the availability of AIREP observations from the 1990s with the initiation of the AMDAR Programme and a decrease in the availability of PILOT wind observations. The number of radiosonde observations increases during the first 20 years of the reanalysis period and decreases again over the following 5 years as reflected in the decrease in the number of humidity observations assimilated (Fig. 3b).

### b. Climatology

The default surface land-cover physiography in HARMONIE-AROME is based on the 1-km-resolution "ECOCLIMAP 2.2" database (Faroux et al. 2013). The land surface characteristics contained in this database define the grid-scale surface SW albedo and LW emissivity. The default surface topography is based on GTOPO30 (USGS 1997), and the clay and sand proportions are based on IUSS Working Group WRB (2006).

HARMONIE-AROME uses monthly "climatologies" of aerosol optical depths (AOD) at 550 nm of land, sea, desert, and urban tropospheric aerosols from the Tegen et al. (1997) climatology along with background stratospheric aerosols in a similar manner to the IFS model (ECMWF 2013). These are distributed among the model levels using the Tanré et al. (1984) climatological vertical profiles for each aerosol type [see Gleeson et al. (2015) and Toll et al. (2016)]. The spectral dependence of AOD, single-scattering albedo, and asymmetry factor  $g$  for each aerosol type is parameterized following Hess et al. (1998). Monthly climatologies of ozone and a fixed composition mixture of  $\text{CO}_2$ ,  $\text{N}_2\text{O}$ ,  $\text{CH}_4$ , and  $\text{O}_2$  are also used.

### c. Boundary conditions

MÉRA forecasts use ERA-Interim (Dee et al. 2011) model-level data as LBCs with the Davies relaxation scheme (Davies 1976) as described in Termonia et al. (2017). Upper boundary conditions are also applied in the same manner at the model top. ERA-Interim

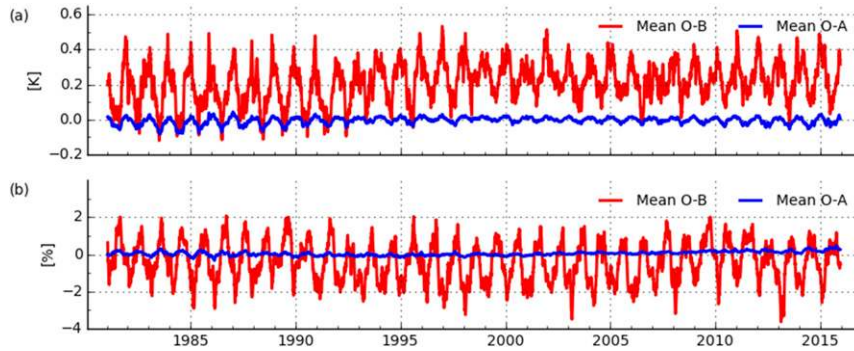


FIG. 4. Mean background departures ( $O - B$ ; red) and analysis departures ( $O - A$ ; blue) for (a)  $T_{2m}$  and (b)  $RH_{2m}$  produced by MÉRA’s OI surface data assimilation system. A 30-day running average is applied.

data are read by the HARMONIE–AROME forecast model every 3 h using one-way nesting. As mentioned in section 2b, ERA-Interim SST and SIC data are interpolated to the MÉRA grid and used as lower boundary conditions.

#### 4. Data assimilation performance

In general, the performance of the surface (OI) and upper-air (3D-Var) data assimilation systems is measured by comparing departure statistics. The background departure is the distance of the background (model state)  $H\mathbf{x}^b$  from the observations  $\mathbf{y}$ . The analysis departure is the distance of the analysis  $H\mathbf{x}^a$  from  $\mathbf{y}$ . Analyses that are closer to the observations than the background are a first indication that a data assimilation system is performing well. These departure statistics are used to assess how well MÉRA assimilated the observations provided to the data assimilation systems. To further evaluate the performance of the 3D-Var data assimilation system, the analyses are compared with independent observations. The quality of the forecast is the ultimate measure of the quality of its initial conditions: the analysis. We did not investigate forecast quality sensitivity to changes in the data assimilation system.

##### a. OI performance

Time series of departure statistics produced by the OI surface data assimilation system have been used to evaluate the performance of the surface analyses produced by MÉRA (Fig. 4). By applying a 30-day running mean to the departure statistics, annual variations in the departure statistics are more easily identified.

Time series of means and standard deviations of departure statistics for  $T_{2m}$  and  $RH_{2m}$  observations used by MÉRA surface analyses indicate that MÉRA surface analyses were consistently closer to these observations

than the background. There is a consistent  $T_{2m}$  background departure throughout the period indicating a cold bias of approximately 0.2 K in the background. This bias has been attributed to the fact that the forecast model produces too much low cloud and fog (Bengtsson et al. 2017; de Rooy 2014). Figure 4a shows a seasonal variation in the magnitude of the mean  $T_{2m}$  background departure with larger biases occurring during the winter. This seasonal variation is less clear in the  $T_{2m}$  standard deviation time series (not shown). Time series of mean departure statistics for  $RH_{2m}$  (Fig. 4b) also show that the analyses were consistently closer to observations, with a moist background bias in the summer and a dry bias in the winter.

##### b. 3D-Var performance

Departure statistics have been used to evaluate the performance of MÉRA’s 3D-Var data assimilation system in the same way as the assimilation of surface observations. The 3D-Var updates geopotential using surface observations of pressure. Time series of mean departures are shown in Fig. 5a. Analyses of geopotential are closer to observed values than the background with a reduction in the magnitude of departures when a greater number of SYNOP and AIREP observations are assimilated later in the reanalysis period. Similar results can be seen for temperature observations from aircraft (Figs. 5b,c). The quality of (mainly AMDAR) aircraft observations in the lower atmosphere (below 700 hPa) is consistent (Fig. 5b) with average values of observed minus analyzed temperature departures close to 0 K. Background and analysis departure time series for aircraft observations of temperature above 400 hPa (Fig. 5c) indicate that, in general, 3D-Var performs well for the assimilation of aircraft temperature observations. However, the introduction of AMDAR observations in the 1990s resulted in an increase in mean background departure values

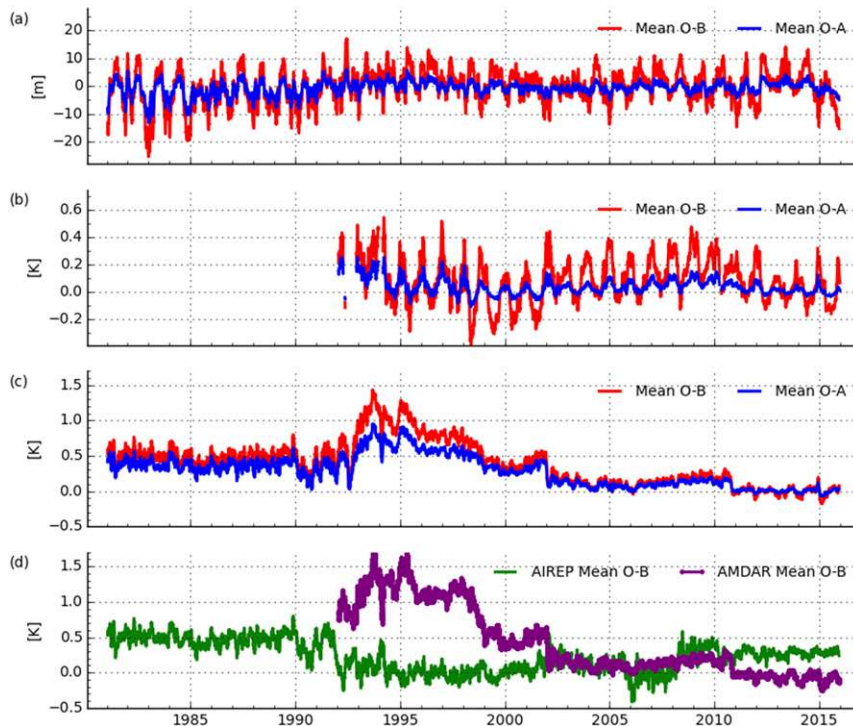


FIG. 5. Mean background departures ( $O - B$ ; red) and analysis departures ( $O - A$ ; blue) for (a) SYNOP geopotential, (b) aircraft (AIREP and AMDAR) temperatures below 700 hPa, and (c) aircraft temperatures above 400 hPa produced by MÉRA's 3D-Var. (d) The  $O - B$  values for AIREP reports (green) and AMDAR reports (purple) above 400 hPa. A 30-day running average is applied.

(1993–98) above 400 hPa (Fig. 5c,d). These larger departure values, for this period, are due to AMDAR temperature observations with gross errors not being rejected by the 3D-Var quality control software. These erroneous observations were from specific aircraft that produced the reports. The fraction of aircraft with these biases decreases significantly after this period. There is also a noticeable shift in the aircraft temperature departure values in 2002 that coincides with a drop in data availability as mentioned in section 3a. The quality of AMDAR observations is discussed further in Petersen (2016).

Background and analysis departures for radiosonde temperature and humidity observations are shown in Fig. 6. Analyses of temperature appear to perform well with departures smaller than the background departures (Figs. 6a,b). However, known biases present in radiosonde observations are well documented (Haimberger 2007; Haimberger and Andrae 2011). Sources of such biases include instrument type, reporting practices, and radiative heating in the upper troposphere. Radiosonde observations are assimilated by MÉRA as presented in the MARS archive with no corrections applied. Temperature biases caused by radiative heating can be identified by subtracting midnight background departures ( $O - B_{00}$ )

from midday background departure ( $O - B_{12}$ ) values. Such biases seem to be present for radiosonde data before 1990 above 100 hPa (Fig. 7a). The temperature radiation bias calculated for the Valentia radiosonde at 100 hPa is shown in Fig. 7b. Use of a homogenized radiosonde dataset such as Radiosonde Observation Correction Using Reanalyses (RAOBCORE) or Radiosonde Innovation Composite Homogenization (RICH) (Haimberger et al. 2012) would improve the quality of analyses in the upper troposphere. Radiosonde observations of humidity above 300 hPa are not assimilated by MÉRA because they were deemed to be of insufficient quality. Time series of standard deviations of humidity background and analysis departures (Figs. 6c,d) suggest that analyses of humidity below 300 hPa are of good quality.

Analysis performance has been further verified using geopotential height observations from TEMP reports. These observations are not assimilated and, as such, can be classified as being independent of the reanalysis data assimilation process. Figure 8 shows a time series of the average differences between root-mean-square error (RMSE) of MÉRA background geopotential height values [ $\text{RMSE}(O - B)$ ] and analysis geopotential height values [ $\text{RMSE}(O - A)$ ]. Positive values of these



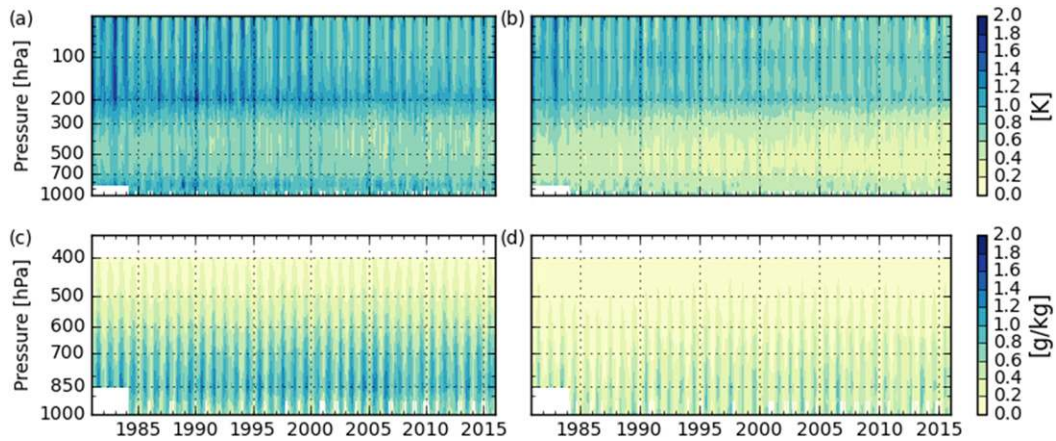


FIG. 6. Radiosonde temperature (a) background departures and (b) analysis departures at standard pressure levels. The lighter yellow colors indicate departure values closer to zero (i.e., model temperature closer to observed temperatures). (c),(d) The reduction in specific humidity standard deviation. A 30-day running average is applied. White areas indicate missing data.

differences indicate lower RMSE( $O - A$ ) values. On average, MÉRA’s 3D-Var improves the model state above 700 hPa by up to 10 m with some brief periods (before 1990 and in 2007) during which the average quality is slightly degraded above 200 hPa by 3D-Var. These periods for which the analysis degrades the model state may be due to radiosonde temperature observation biases that have already been described.

**5. Reanalysis performance**

The quality of near-surface parameters produced by the MÉRA reanalysis and its ability to recreate past weather extremes was measured against conventional observations. MÉRA data have been compared with the ERA-Interim (79-km grid) and UERRA HARMONIE–ALADIN (11-km grid) reanalysis datasets. The HARMONIE–ALADIN dataset was generated as part of the UERRA project using the same model version as MÉRA and is hereafter referred to as UERRA. Gridded ERA-Interim and UERRA data were retrieved from ECMWF’s MARS archive with point data extracted for the observation locations. Data were extracted at observation locations using bilinear interpolation. A selection of near-surface parameters were validated against in situ SYNOP observations and the quality of precipitation forecasts was assessed by comparison with observations from Met Éireann’s rainfall observation network. Maps of available SYNOP observations for two dates in 1985 and 2015 are shown in Figs. 9a and 9b. There is a noticeable increase in the density of the SYNOP network over the reanalysis period, as already shown in Fig. 3c. Figure 9c shows the typical coverage and density of

daily precipitation observations used to evaluate the reanalysis performance. These observations typically number between 300 and 500 and are the basis of the gridded monthly precipitation observations used to validate monthly accumulations of precipitation produced by MÉRA, ERA-Interim, and UERRA. Observations from rainfall stations on higher ground or in more remote locations are collected on a monthly basis. MÉRA is validated using average error (bias), average standard deviation, and the Heidke skill score (HSS) (Heidke 1926;

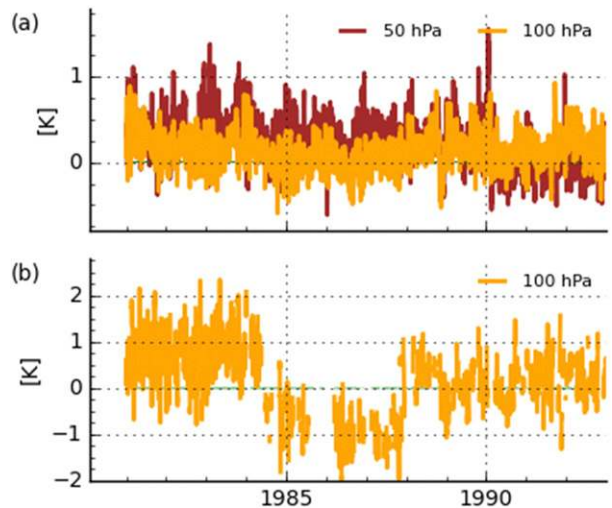


FIG. 7. (a) Radiosonde temperature background departures at 0000 UTC subtracted from 1200 UTC background departures for observations at 50 hPa, shown in brown, and observations at 100 hPa, shown in orange, for all radiosondes observations assimilated by MÉRA. (b) As in (a), but showing Valentia Observatory observations at 100 hPa. A 7-day running average is applied.

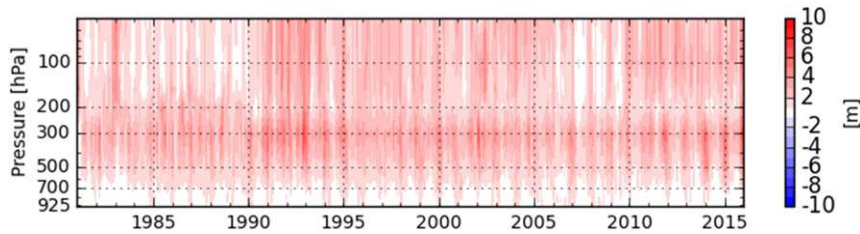


FIG. 8. Average differences between RMSE of background geopotential heights [ $\text{RMSE}(O - B)$ ] and analysis geopotential heights [ $\text{RMSE}(O - A)$ ] compared with observations available in TEMP reports. Positive values (red colors) indicate that  $\text{RMSE}(O - A)$  values are lower than  $\text{RMSE}(O - B)$  and that the analysis values of geopotential height are of improved quality when compared with geopotential height observations.

Hyvärinen 2014) to compare the three reanalysis datasets. The HSS is a categorical skill score with one indicating a perfect forecast and zero indicating no skill.

Particular attention is given to the quality of near-surface (10 m) winds and daily precipitation accumulations. In general, severe weather events in Ireland are related to strong winds produced by Atlantic storms or accumulations of precipitation that lead to winter flooding. An evaluation of MÉRA surface (including spinup) and upper-air parameters is provided in Gleeson et al. (2017).

#### a. Near surface

We have compared MÉRA forecasts of surface pressure with observations from synoptic reports. Figure 10 shows the standard deviation of MÉRA 0000 UTC 0- (analysis), 3-, 6-, 12-, and 24-h forecasts for 1981–2015. The quality of MÉRA forecasts is very consistent, with a general improvement in forecast quality toward the end of the reanalysis period. This improvement can be attributed to the increase in the number of observations assimilated by MÉRA.

To compare MÉRA with other reanalysis datasets, we have verified 3-h forecasts from MÉRA, ERA-Interim,

and UERRA with synoptic observations available within the MÉRA domain (i.e., observations from Ireland, the United Kingdom, and northern France). It was only possible to include 3-h forecasts from the 0000 and 1200 UTC cycles because 3-h forecasts are unavailable for other ERA-Interim forecast cycles.

Verification results are shown for the years 1981–2015 for mean sea level pressure (MSLP) (Fig. 11a) and 2-m temperature (Figs. 11b,c). The figures show the standard deviation of MÉRA, ERA-Interim, and UERRA 3-h forecasts relative to observations where a 3-month running average is applied for both visualization purposes and the identification of any seasonal trends. Overall, the results indicate that MÉRA performs consistently over the time period. It performs similarly to ERA-Interim and UERRA for MSLP (Fig. 11a), with all three reanalyses showing a reduction in the standard deviation of MSLP from about 0.5 hPa at the start of the period (1981–1990) to less than 0.4 hPa near the end (2010–15). MÉRA outperforms ERA-Interim and UERRA (Figs. 11b,c) in terms of the standard deviation of 2-m temperature forecasts. There is an increase in the ERA-Interim and (to a lesser extent) UERRA 2-m

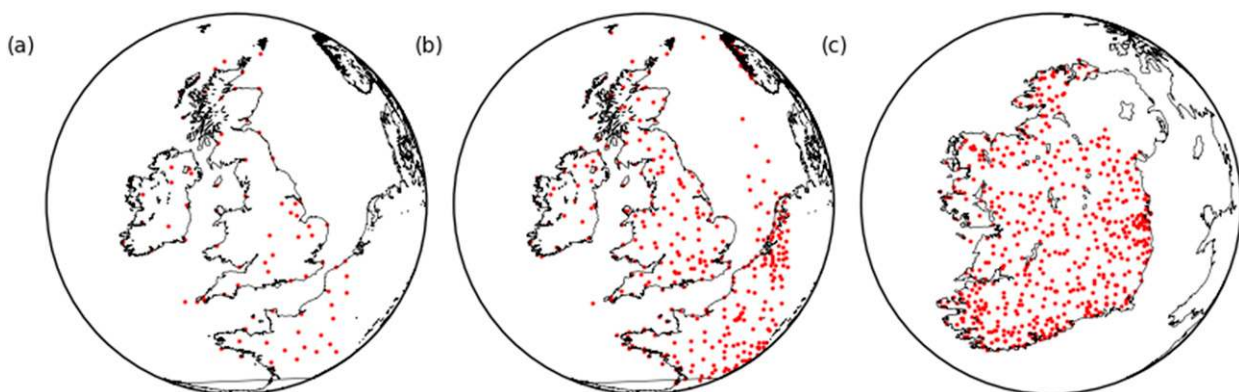


FIG. 9. Typical maps of observations used to validate MÉRA forecasts. SYNOP observations at (a) 1200 UTC 1 Jun 1985 and (b) 1200 UTC 1 Jun 2015. (c) Map of daily precipitation observations produced by Met Éireann for 1 Jun 1985.

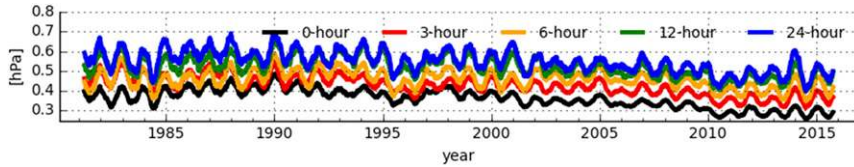


FIG. 10. Standard deviations of MSLP 3- (red), 6- (orange), 12- (green), and 24-h (blue) forecasts produced by MÉRA 0000 UTC runs compared with observations from SYNOP reports. A 3-month running average is applied.

temperature standard deviation values from about 1990. The number of observations available from the SYNOP network for verification increased from that time with many new observation sites positioned near coasts or on higher ground (Fig. 9). The number of SYNOP stations sited above 250m increased from 5 in 1985 to 42 in 2015. It was possible to correct for model orography errors using an adiabatic lapse-rate correction. This correction was applied to ERA-Interim (light blue; Fig. 11b) and UERRA (light green; Fig. 11c) forecasts for fairer comparison. The lapse-rate correction improves ERA-Interim standard deviations from about 1.7 to 1.5K after 1990 but has little effect, on average, when applied to

UERRA 3-h forecasts. In terms of 2-m temperature biases, identified in section 4, MÉRA outperforms ERA-Interim and UERRA, with a running mean bias of  $\pm 0.2\text{K}$  as compared with  $\pm 0.4\text{K}$  and  $\pm 0.6\text{K}$  for UERRA and ERA-Interim, respectively. Both MÉRA and UERRA used ERA-Interim LBCs, which place constraints on larger atmospheric scales. Thus, the differences in biases and standard deviations in MSLP for MÉRA, UERRA, and ERA-Interim are small.

*b. Winds*

Figure 11d shows the standard deviation of MÉRA, ERA-Interim, and UERRA 3-h forecasts relative to the

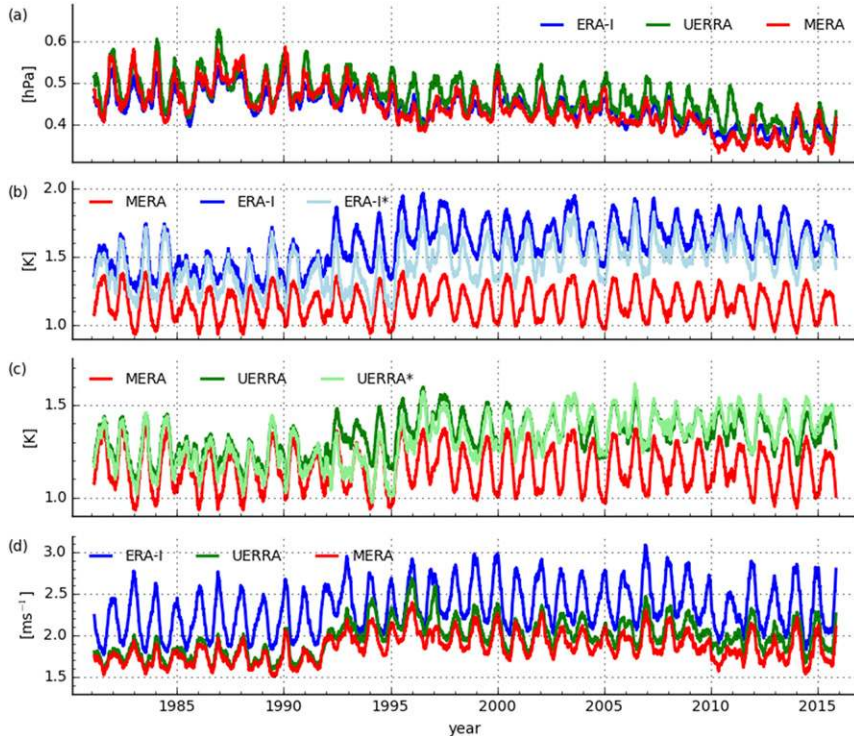


FIG. 11. (a) Standard deviations of MÉRA (red), ERA-Interim (blue), and UERRA (green) 3-h forecasts of MSLP. (b) Standard deviations of ERA-Interim (blue), corrected ERA-Interim (light-blue, ERA-I\*), and MÉRA (red) 3-h forecasts of  $T_{2m}$ . (c) Standard deviations of UERRA (green), corrected UERRA (light green, UERRA\*), and MÉRA 3-h forecasts of  $T_{2m}$ . (d) As in (a), but for 10-m wind speeds. A 3-month running average is applied.

corresponding synoptic observations. Again, a 3-month averaging is applied. A similar increase in 10-m wind speed standard deviations (as noted in section 5a) is seen for all datasets after 1990. The results of this comparison show that MÉRA performs consistently for the re-analysis period. According to this measure, MÉRA outperforms both ERA-Interim and UERRA. Again, this improvement can be attributed to the improved orographic representation that comes with higher model resolution.

However, this measure of near-surface wind quality applies a lot of averaging to the data, and information on extremes is not clear from these statistics. Figure 12a shows the relative frequency distribution of 10-m wind speeds from 3-h forecasts of 0000 and 1200 UTC model runs in comparison with observations from (land) SYNOP reports. The bins were chosen so that their cut-offs coincided with the limits of the wind speed ranges on the Beaufort scale. ERA-Interim overpredicts wind speeds at 10 m over  $5 \text{ m s}^{-1}$  and, as a consequence of this shifted wind speed distribution, matches well with higher wind speeds (over  $15 \text{ m s}^{-1}$ ). UERRA overpredicts lower wind speeds ( $5\text{--}10 \text{ m s}^{-1}$ ) and underpredicts higher wind speeds (over  $10 \text{ m s}^{-1}$ ). MÉRA shows similar characteristics to UERRA with an overprediction of lower wind speeds and an underprediction of higher wind speeds. The relative frequency of MÉRA wind speeds matches the relative frequency of observed wind speeds for all of the data bins. The HSS for wind speeds for the period 1981–2015 are shown in Fig. 12b. The HSS was calculated for all 3-h forecasts from 0000 and 1200 UTC model runs (1981–2015) for the three datasets. While there is little difference between the HSS values for MÉRA and UERRA for lower winds speeds, the forecast skill, as measured by the HSS, of MÉRA over ERA-Interim and UERRA can be clearly be seen for higher winds speeds (over  $10 \text{ m s}^{-1}$ ).

### c. Precipitation

Precipitation forecasts produced by MÉRA, ERA-Interim, and UERRA were compared with observations of 24-h accumulations of precipitation recorded by Met Éireann's network of (approximately 400) rainfall stations (0900–0900 UTC). For MÉRA the accumulations from the 9- and 33-h forecasts from the 0000 UTC runs were used to calculate the 24-h accumulations for the same validity periods as the observations. The 30-h ERA-Interim forecasts only cover the period from 0000 to 0600 UTC the following day. For this reason, the 0900–0900 UTC precipitation forecasts shown for ERA-Interim consist of the sum of the 9–24-h accumulation and the 0–9-h accumulation of the following day. UERRA is similar to ERA-Interim in that 24- and 9-h

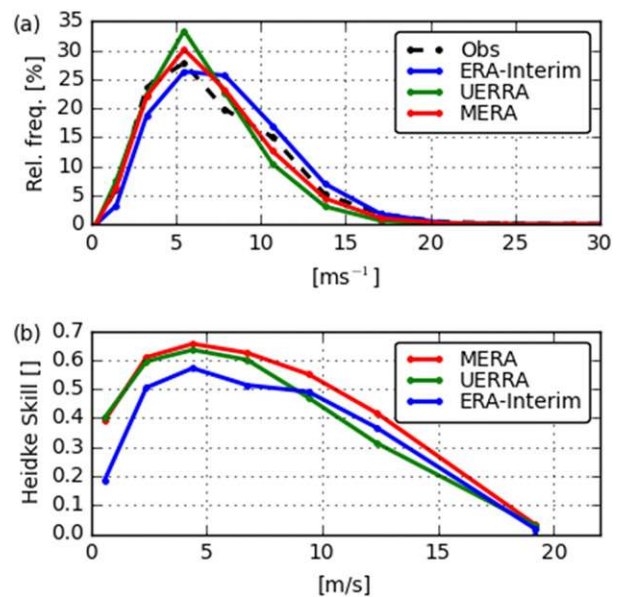


FIG. 12. (a) Relative frequency of observed (black), ERA-Interim (blue), UERRA (green), and MÉRA (red) 10-m wind speeds. (b) HSSs for ERA-Interim, UERRA, and MÉRA forecasts. Both (a) and (b) use forecasts and observations for the period 1981–2015.

forecasts had to be used to generate the 0900–0900 UTC precipitation totals. The construction of daily accumulations of precipitation in this manner has been shown to produce good-quality estimates (Landelius et al. 2016), once spinup forecast data are not used. For MÉRA, a single long forecast each day was produced for practical reasons.

Figure 13 shows areal comparisons of monthly precipitation [for winter: December–February (DJF)] averaged over the period 1981–2015. The MÉRA, UERRA, and ERA-Interim datasets were compared to gridded observations of monthly accumulations of precipitation; the observations were projected onto each model domain by conservatively averaging the accumulations in each model grid box, in order to make appropriate comparisons between each model and the observations. Table 3 lists statistics comparing seasonal biases and standard deviations for MÉRA, UERRA, and ERA-Interim precipitation accumulations. Whereas MÉRA biases are smallest for the autumn and winter seasons, the higher-resolution reanalyses, MÉRA and UERRA, overpredict spring and summer precipitation. ERA-Interim precipitation biases for spring and summer are very close to 0 mm. The plots in the first column of Fig. 13 show the monthly observed DJF precipitation averaged over the period 1981–2015 on the ERA-Interim, UERRA, and MÉRA grids; the plots in the second columns show the

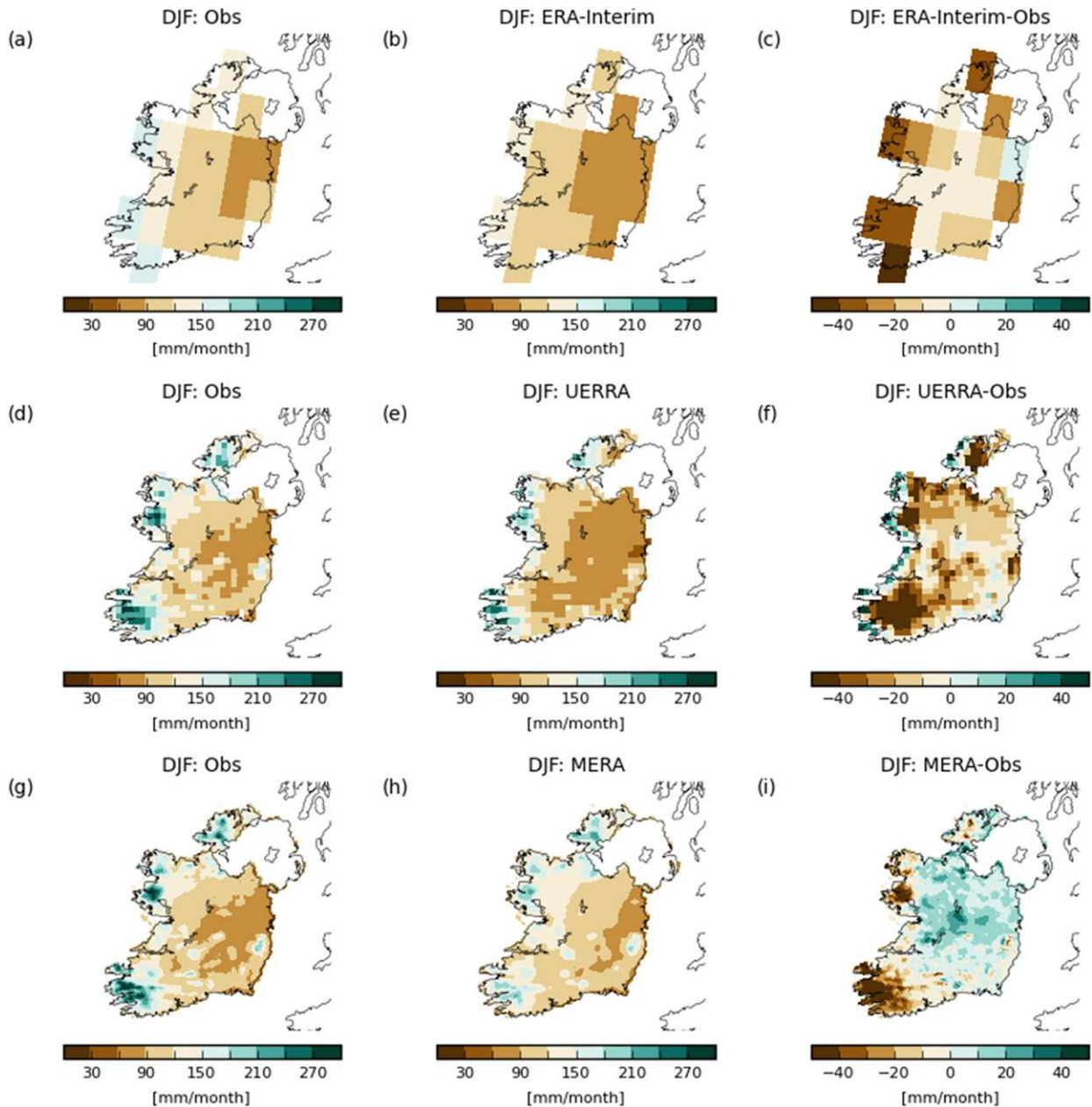


FIG. 13. Monthly mean DJF precipitation for the period 1981–2015. Observations projected onto (a) the ERA-Interim grid, (b) ERA-Interim, and (c) ERA-Interim minus observed. (d)–(f) As in (a)–(c), but for UERRA. (g)–(i) As in (a)–(c), but for MÉRA.

corresponding precipitation from each model while the third column shows the difference between each model and the observations. The coarse ERA-Interim grid mainly underpredicts monthly precipitation, particularly over mountainous areas where the biases are on the order of 50 mm. Both UERRA and MÉRA also underpredict the precipitation over mountains because of mismatches in orography; the 2.5- and 11-km grid spacings cannot account for mountain peaks contained

within a grid box. UERRA underpredicts precipitation over most of the country whereas MÉRA overpredicts the total by ~10–20 mm, with the exception being over high ground. As anticipated, the higher-resolution MÉRA shows a noticeable improvement over the coarser-resolution ERA-Interim and UERRA reanalyses, which underestimate precipitation over the MÉRA domain by up to ~50 mm month<sup>-1</sup>. As before, this can be attributed to model resolution and

TABLE 3. Precipitation statistics (1981–2015) for MÉRA and UERRA listing seasonal biases and standard deviations when compared with gridded precipitation accumulation observations. Winter is defined as December–February, spring as March–May, summer as June–August, and autumn as September–November.

	MÉRA		UERRA		ERA-Interim	
	Bias (mm)	Std dev (mm)	Bias (mm)	Std dev (mm)	Bias (mm)	Std dev (mm)
Winter	−0.5	19.8	−18.3	20.9	−18.0	13.2
Spring	8.6	13.4	20.9	12.5	0.2	12.3
Summer	1.4	15.1	32.3	10.3	−0.2	13.3
Autumn	−2.8	19.2	−12.0	16.7	−17.1	12.2

the mesoscale physics parameterizations that resolve convection in MÉRA. The bias patterns for MÉRA are similar for each season (not shown), that is, negative biases over high ground and positive biases elsewhere.

Figure 14a shows the relative frequency distribution of monthly mean DJF 0900–0900 UTC precipitation accumulations for the models and observations. ERA-Interim overpredicts light precipitation and underpredicts extremes. MÉRA and UERRA both match the relative frequency distribution quite well for higher accumulations with MÉRA underpredicting moderate (5 mm) daily accumulations. As with the analysis of 10-m wind speeds, we have calculated the HSS for 24-h accumulated precipitation forecasts for each of the three reanalysis datasets, ERA-Interim, UERRA, and MÉRA, to measure their forecast skill (Fig. 14b). There is little difference in skill for lower accumulations (less than 10 mm), with MÉRA performing better than UERRA for more extreme (greater than 25 mm) precipitation accumulations.

We use the 9- and 33-h precipitation forecasts from the 0000 UTC MÉRA runs to determine the 0900–0900 UTC 24-h rainfall accumulations; that is, we neglected the first few hours of rainfall forecasts, which are deemed to be inaccurate as the model is still spinning up. This assumption is justified by Fig. 15, in which the 24-h accumulations are compared with those computed using successive 3-h forecasts covering the same periods. At first glance, it seems that using the 3-h forecasts reduces the biases over inland and nonmountainous regions (Fig. 15c). However, this apparent improvement arises because the 3-h forecasts produce a much drier climatology at all locations (see Fig. 15d).

## 6. Conclusions and discussion

A basic analysis of some of the output from MÉRA was presented in Gleeson et al. (2017) and is extended in this paper, in particular in relation to data assimilation and extremes of wind and precipitation. We have shown that the HARMONIE–AROME data

assimilation system and forecast model perform well and consistently when compared with point observations. MÉRA's advantage over UERRA, one of the highest-resolution regional reanalyses for Europe, is also illustrated for a selection of surface parameters and we show that, using appropriate skill scores, MÉRA is better at recreating extremes of wind and precipitation. ERA-Interim data have been included in these comparison for completeness.

MÉRA is the highest-resolution, regional reanalysis dataset for Ireland and the United Kingdom and is being widely used in academia and industry. The ongoing analysis and use of MÉRA data will promote improvements to Met Éireann's operational NWP suite. The next generation of regional reanalyses within the Copernicus Climate Change Services has commenced with Production of a Regional Reanalysis for Europe (PRECISE) producing a 5-km reanalysis for Europe and the Copernicus Arctic Regional Reanalysis (CARRA)

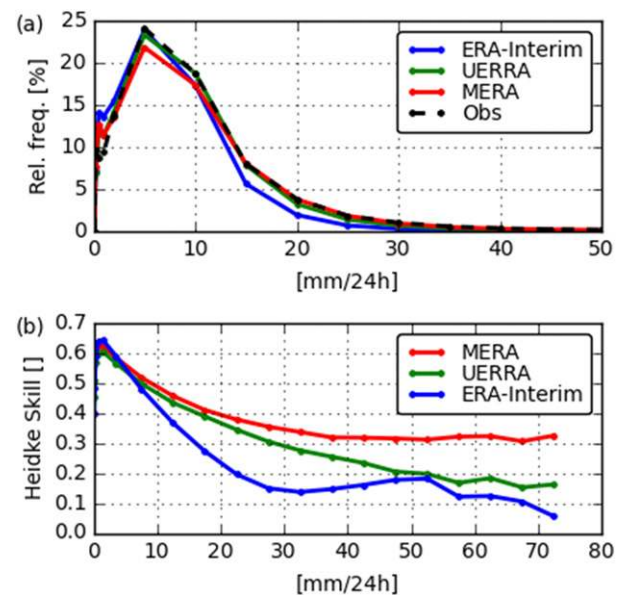


FIG. 14. As in Fig. 12, but for 0900–0900 UTC 24-h precipitation accumulations.

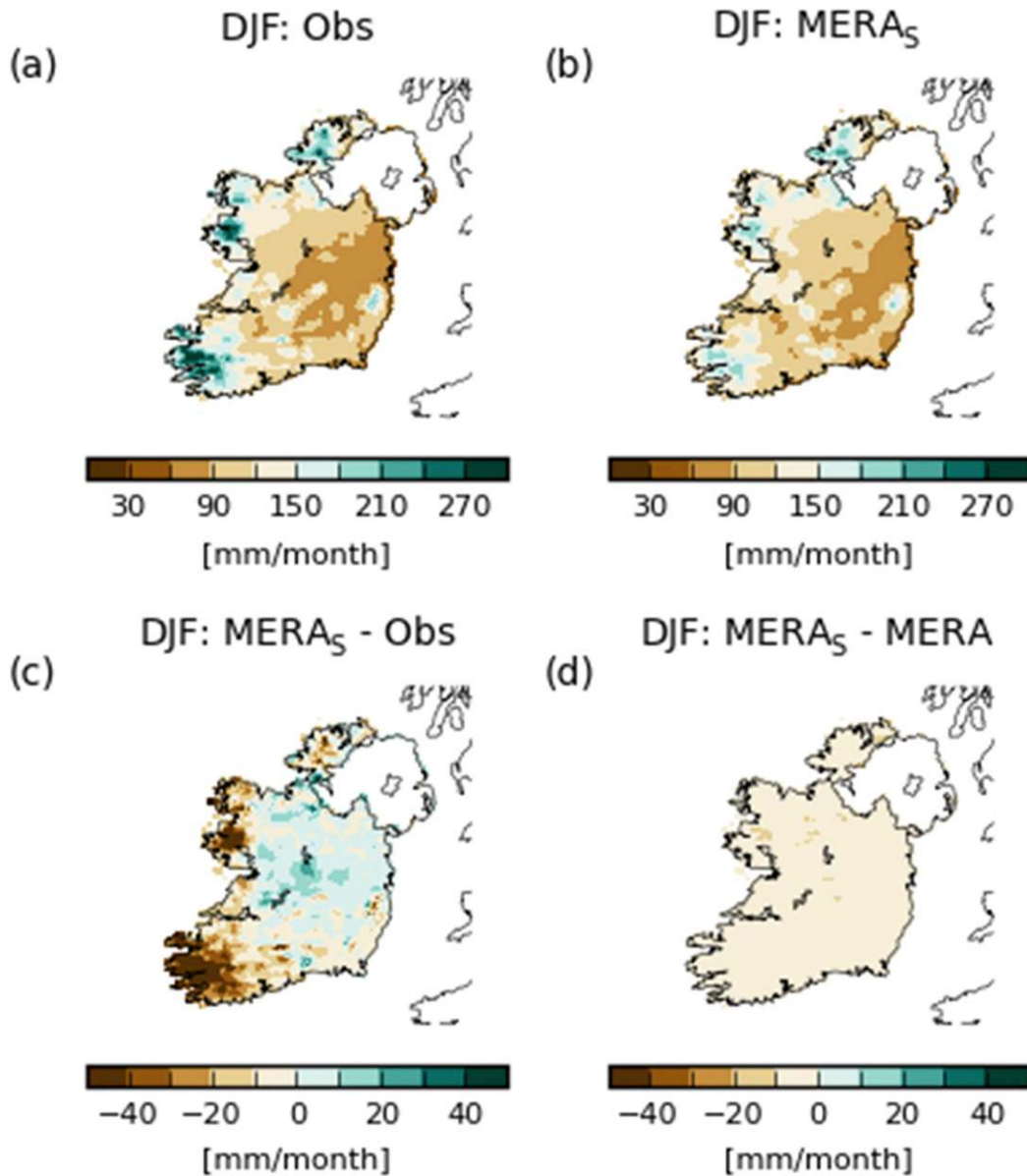


FIG. 15. Monthly mean DJF precipitation for the period 1981–2015. (a) Observations projected on the MÉRA grid. (b) MÉRA data for which the 0900–0900 UTC 24-h accumulations were calculated by summing the accumulations from relevant successive 3-h forecasts. (c) MÉRA (sum of 3-h forecasts) minus observed. (d) MÉRA (sum of 3-h forecasts) minus MÉRA using 24-h forecasts.

producing a 2.5-km reanalysis for two Arctic domains. Production of a 12-km regional reanalysis for Australia [Bureau of Meteorology Atmospheric High-Resolution Regional Reanalysis for Australia (BARRA)], with multiple mesoscale 1.5-km reanalyses driven by the 12-km data, has commenced. These, and other future regional reanalyses, will benefit from the enhanced use of observations as well as developments in reanalysis methods such as improvements in data assimilation algorithms and the use of ensemble techniques.

A future regional reanalysis for Ireland would also benefit from these developments as well as the use of LBCs from future global reanalyses.

*Acknowledgments.* We acknowledge the support of the HIRLAM and ALADIN programs. We thank Bing Li and Ray McGrath for their help in preparing the observations used in the MÉRA project and Séamus Walsh for providing the gridded precipitation observations.

## REFERENCES

- Arriola, J. S., M. Lindskog, S. Thorsteinsson, and J. Bojarova, 2016: Variational bias correction of GNSS ZTD in the HARMONIE modeling system. *J. Appl. Meteor. Climatol.*, **55**, 1259–1276, <https://doi.org/10.1175/JAMC-D-15-0137.1>.
- Belamari, S., 2005: Report on uncertainty estimates of an optimal bulk formulation for surface turbulent fluxes. Marine Environment and Security for the European Area—Integrated Project (MERSEA IP), European Commission Deliverable D, Vol. 4, 29 pp. [The report is available upon request from the corresponding author.]
- Bénard, P., J. Vivoda, J. Mašek, P. Smolíková, K. Yessad, C. Smith, R. Brožková, and J.-F. Geleyn, 2010: Dynamical kernel of the Aladin-NH spectral limited-area model: Revised formulation and sensitivity experiments. *Quart. J. Roy. Meteor. Soc.*, **136**, 155–169, <https://doi.org/10.1002/qj.522>.
- Bengtsson, L., S. Tijm, F. Váňa, and G. Svensson, 2012: Impact of flow-dependent horizontal diffusion on resolved convection in AROME. *J. Appl. Meteor. Climatol.*, **51**, 54–67, <https://doi.org/10.1175/JAMC-D-11-032.1>.
- , and Coauthors, 2017: The HARMONIE–AROME model configuration in the ALADIN–HIRLAM NWP system. *Mon. Wea. Rev.*, **145**, 1919–1935, <https://doi.org/10.1175/MWR-D-16-0417.1>.
- Bollmeyer, C., and Coauthors, 2015: Towards a high-resolution regional reanalysis for the European CORDEX domain. *Quart. J. Roy. Meteor. Soc.*, **141**, 1–15, <https://doi.org/10.1002/qj.2486>.
- Boone, A., J.-C. Calvet, and J. Noilhan, 1999: Inclusion of a third soil layer in a land surface scheme using the force–restore method. *J. Appl. Meteor.*, **38**, 1611–1630, [https://doi.org/10.1175/1520-0450\(1999\)038<1611:IOATSL>2.0.CO;2](https://doi.org/10.1175/1520-0450(1999)038<1611:IOATSL>2.0.CO;2).
- Bougeault, P., and P. Lacarrère, 1989: Parameterization of orography-induced turbulence in a mesobeta-scale model. *Mon. Wea. Rev.*, **117**, 1872–1890, [https://doi.org/10.1175/1520-0493\(1989\)117<1872:POOITI>2.0.CO;2](https://doi.org/10.1175/1520-0493(1989)117<1872:POOITI>2.0.CO;2).
- Bouteloup, Y., Y. Seity, and E. Bazile, 2011: Description of the sedimentation scheme used operationally in all Météo-France NWP models. *Tellus*, **63A**, 300–311, <https://doi.org/10.1111/j.1600-0870.2010.00484.x>.
- Bromwich, D., Y.-H. Kuo, M. Serreze, J. Walsh, L.-S. Bai, M. Barlage, K. Hines, and A. Slater, 2010: Arctic system reanalysis: Call for community involvement. *Eos, Trans. Amer. Geophys. Union*, **91** (2), 13–14, <https://doi.org/10.1029/2010EO020001>.
- Brousseau, P., L. Berre, F. Bouttier, and G. Desroziers, 2011: Background-error covariances for a convective-scale data-assimilation system: AROME-France 3D-Var. *Quart. J. Roy. Meteor. Soc.*, **137**, 409–422, <https://doi.org/10.1002/qj.750>.
- Bubnová, R., G. Hello, P. Bénard, and J.-F. Geleyn, 1995: Integration of the fully elastic equations cast in the hydrostatic pressure terrain-following coordinate in the framework of the ARPEGE/Aladin NWP system. *Mon. Wea. Rev.*, **123**, 515–535, [https://doi.org/10.1175/1520-0493\(1995\)123<0515:IOFEE>2.0.CO;2](https://doi.org/10.1175/1520-0493(1995)123<0515:IOFEE>2.0.CO;2).
- Charnock, H., 1955: Wind stress on a water surface. *Quart. J. Roy. Meteor. Soc.*, **81**, 639–640, <https://doi.org/10.1002/qj.49708135027>.
- Courtier, P., and Coauthors, 1998: The ECMWF implementation of three-dimensional variational assimilation (3D-Var). I: Formulation. *Quart. J. Roy. Meteor. Soc.*, **124**, 1783–1807, <https://doi.org/10.1002/qj.49712455002>.
- Cuxart, J., P. Bougeault, and J.-L. Redelsperger, 2000: A turbulence scheme allowing for mesoscale and large-eddy simulations. *Quart. J. Roy. Meteor. Soc.*, **126**, 1–30, <https://doi.org/10.1002/qj.49712656202>.
- Dahlgren, P., 2013: A comparison of two large scale blending methods: Jk and LSMIXBC. Norwegian Meteorological Institute–Swedish Meteorological and Hydrological Institute MetCoOp Memo. 2, 10 pp., <http://metcoop.org/memo/2013/02-2013-METCOOP-MEMO.PDF>.
- , T. Landelius, P. Källberg, and S. Gollvik, 2016: A high-resolution regional reanalysis for Europe. Part 1: Three-dimensional reanalysis with the regional High-Resolution Limited-Area Model (HIRLAM). *Quart. J. Roy. Meteor. Soc.*, **142**, 2119–2131, <https://doi.org/10.1002/qj.2807>.
- Davies, H. C., 1976: A lateral boundary formulation for multi-level prediction models. *Quart. J. Roy. Meteor. Soc.*, **102**, 405–418, <https://doi.org/10.1002/qj.49710243210>.
- Dee, D. P., and Coauthors, 2011: The ERA-Interim reanalysis: Configuration and performance of the data assimilation system. *Quart. J. Roy. Meteor. Soc.*, **137**, 553–597, <https://doi.org/10.1002/qj.828>.
- de Rooy, W., 2014: The fog above sea problem: Part 1 analysis. *Joint ALADIN-HIRLAM Newsletter*, No. 2, Météo-France, Centre National de Recherches Meteorologiques, Toulouse, France, 9–15, [http://www.umr-cnrm.fr/aladin/IMG/pdf/ah\\_newsletter\\_2\\_april\\_2014\\_1\\_.pdf](http://www.umr-cnrm.fr/aladin/IMG/pdf/ah_newsletter_2_april_2014_1_.pdf).
- , and A. P. Siebesma, 2008: A simple parameterization for detrainment in shallow cumulus. *Mon. Wea. Rev.*, **136**, 560–576, <https://doi.org/10.1175/2007MWR2201.1>.
- Desroziers, G., L. Berre, B. Chapnik, and P. Poli, 2005: Diagnosis of observation, background and analysis error statistics in observation space. *Quart. J. Roy. Meteor. Soc.*, **131**, 3385–3396, <https://doi.org/10.1256/qj.05.108>.
- ECMWF, 2003: Part IV: Physical processes. *IFS Documentation CY25RI*, ECMWF, 166 pp., <https://www.ecmwf.int/sites/default/files/elibrary/2003/13280-part-iv-physical-processes.pdf>.
- , 2013: Part IV: Physical processes. *IFS Documentation CY38RI*, ECMWF, 189 pp., <https://www.ecmwf.int/en/elibrary/9245-part-iv-physical-processes>.
- European Commission, 2017: Uncertainties in Ensembles of Regional Reanalyses. European FP7 Project, European Commission, <http://www.uerra.eu>.
- Faroux, S., A. Kaptué Tchuenté, J.-L. Roujean, V. Masson, E. Martin, and P. L. Moigne, 2013: ECOCLIMAP-II/Europe: A twofold database of ecosystems and surface parameters at 1 km resolution based on satellite information for use in land surface, meteorological and climate models. *Geosci. Model Dev.*, **6**, 563–582, <https://doi.org/10.5194/gmd-6-563-2013>.
- Fischer, C., T. Montmerle, L. Berre, L. Auger, and S. E. Ştefănescu, 2005: An overview of the variational assimilation in the ALADIN/France numerical weather-prediction system. *Quart. J. Roy. Meteor. Soc.*, **131**, 3477–3492, <https://doi.org/10.1256/qj.05.115>.
- Fleming, R., T. Kaneshige, and W. McGovern, 1979: The Global Weather Experiment: 1. The observational phase through the first special observing period. *Bull. Amer. Meteor. Soc.*, **60**, 649–661, [https://doi.org/10.1175/1520-0477\(1979\)060<0649:TGWETO>2.0.CO;2](https://doi.org/10.1175/1520-0477(1979)060<0649:TGWETO>2.0.CO;2).
- Gelaro, R., and Coauthors, 2017: The Modern-Era Retrospective Analysis for Research and Applications, version 2 (MERRA-2). *J. Climate*, **30**, 5419–5454, <https://doi.org/10.1175/JCLI-D-16-0758.1>.
- Giard, D., and E. Bazile, 2000: Implementation of a new assimilation scheme for soil and surface variables in a global NWP model. *Mon. Wea. Rev.*, **128**, 997–1015, [https://doi.org/10.1175/1520-0493\(2000\)128<0997:IOANAS>2.0.CO;2](https://doi.org/10.1175/1520-0493(2000)128<0997:IOANAS>2.0.CO;2).
- Gibson, J., P. Källberg, S. Uppala, A. Hernandez, A. Nomura, and E. Serrano, 1997: ERA description. ECMWF ERA Report



- Series No. 1, 72 pp., <https://www.ecmwf.int/en/elibrary/9584-era-description>.
- Gleeson, E., C. O'Hara, S. Walsh, and S. Duffy, 2015: To what extent does the large temporal variability in Irish precipitation mask underlying trends. *Met Éireann Tech. Note* 63, 26 pp., <http://hdl.handle.net/2262/74730>.
- , E. Whelan, and J. Hanley, 2017: Met Éireann high resolution reanalysis for Ireland. *Adv. Sci. Res.*, **14**, 49–61, <https://doi.org/10.5194/asr-14-49-2017>.
- Guidard, V., and C. Fischer, 2008: Introducing the coupling information in a limited-area variational assimilation. *Quart. J. Roy. Meteor. Soc.*, **134**, 723–735, <https://doi.org/10.1002/qj.215>.
- Haimberger, L., 2007: Homogenization of radiosonde temperature time series using innovation statistics. *J. Climate*, **20**, 1377–1403, <https://doi.org/10.1175/JCLI4050.1>.
- , and U. Andrae, 2011: Radiosonde temperature bias correction in ERA-Interim. ECMWF ERA Report Series, No. 8, 17 pp., <https://www.ecmwf.int/en/elibrary/9737-radiosonde-temperature-bias-correction-era-interim>.
- , C. Tavolato, and S. Sperka, 2012: Homogenization of the Global Radiosonde Temperature Dataset through combined comparison with reanalysis background series and neighboring stations. *J. Climate*, **25**, 8108–8131, <https://doi.org/10.1175/JCLI-D-11-00668.1>.
- Heidke, P., 1926: Berechnung des Erfolges und der Gute der Windstarkevorhersagen im Sturmwarnungsdienst (Measures of success and goodness of wind force forecasts by the gale-warning service). *Geogr. Ann.*, **8**, 301–349.
- Hersbach, H., and D. Dee, 2016: ERA5 reanalysis is in production. *ECMWF Newsletter*, No. 147, ECMWF, Reading, United Kingdom, <https://www.ecmwf.int/en/elibrary/16299-newsletter-no-147-spring-2016>.
- , C. Peubey, A. Simmons, P. Poli, D. Dee, and P. Berrisford, 2013: ERA-20CM: A twentieth century atmospheric model ensemble. ECMWF ERA Report Series, No. 16, 44 pp., <https://www.ecmwf.int/en/elibrary/9870-era-20cm-twentieth-century-atmospheric-model-ensemble>.
- Hess, M., P. Koepke, and I. Schult, 1998: Optical properties of aerosols and clouds: The software package OPAC. *Bull. Amer. Meteor. Soc.*, **79**, 831–844, [https://doi.org/10.1175/1520-0477\(1998\)079<0831:OPOAAC>2.0.CO;2](https://doi.org/10.1175/1520-0477(1998)079<0831:OPOAAC>2.0.CO;2).
- Hyyärinen, O., 2014: A probabilistic derivation of Heidke skill score. *Wea. Forecasting*, **29**, 177–181, <https://doi.org/10.1175/WAF-D-13-00103.1>.
- IUSS Working Group WRB, 2006: World Reference Base for Soil Resources 2006: A framework for international classification, correlation and communication. U.N. Food and Agriculture Organization World Soil Resources Rep. 103, <http://www.fao.org/3/a-a0510e.pdf>.
- Kaiser-Weiss, A., F. Kaspar, V. Heene, M. Borsche, D. Tan, P. Poli, A. Obregon, and H. Gregow, 2015: Comparison of regional and global reanalysis near-surface winds with station observations over Germany. *Adv. Sci. Res.*, **12**, 187–198, <https://doi.org/10.5194/asr-12-187-2015>.
- Klein Tank, A. M. G., 2010: EURO4M: Monitoring weather and climate extremes in Europe. *10th EMS Annual Meeting–10th European Conf. on Applications of Meteorology*, Vol. 1, Zürich, Switzerland, European Meteorological Society, 202, <http://meetings.copernicus.org/ems2010>.
- Kobayashi, S., and Coauthors, 2015: The JRA-55 Reanalysis: General specifications and basic characteristics. *J. Meteor. Soc. Japan*, **93**, 5–48, <https://doi.org/10.2151/jmsj.2015-001>.
- Lafore, J. P., and Coauthors, 1998: The Meso-NH atmospheric simulation system. Part I: Adiabatic formulation and control simulations. *Ann. Geophys.*, **16**, 90–109, <https://doi.org/10.1007/s00585-997-0090-6>.
- Landelius, T., P. Dahlgren, S. Gollvik, A. Jansson, and E. Olsson, 2016: A high-resolution regional reanalysis for Europe. Part 2: 2D analysis of surface temperature, precipitation and wind. *Quart. J. Roy. Meteor. Soc.*, **142**, 2132–2142, <https://doi.org/10.1002/qj.2813>.
- Laprise, R., 1992: The Euler equations of motion with hydrostatic pressure as an independent variable. *Mon. Wea. Rev.*, **120**, 197–207, [https://doi.org/10.1175/1520-0493\(1992\)120<0197:TEEOMW>2.0.CO;2](https://doi.org/10.1175/1520-0493(1992)120<0197:TEEOMW>2.0.CO;2).
- Lascaux, F., E. Richard, and J.-P. Pinty, 2006: Numerical simulations of three different MAP IOPs and the associated microphysical processes. *Quart. J. Roy. Meteor. Soc.*, **132**, 1907–1926, <https://doi.org/10.1256/qj.05.197>.
- Lindskog, M., S. Thorsteinsson, and U. Andrae, 2010: A comparison of HARMONIE and HIRLAM 3-dimensional variational data assimilation. *HIRLAM Newsletter*, No. 56, HIRLAM, De Bilt, Netherlands, 3–11, [http://www.hirlam.org/index.php/component/docman/cat\\_view/77-hirlam-official-publications/78-hirlam-newsletters/240-hirlam-newsletter-no-56](http://www.hirlam.org/index.php/component/docman/cat_view/77-hirlam-official-publications/78-hirlam-newsletters/240-hirlam-newsletter-no-56).
- Luhamaa, A., K. Kimmel, A. Männik, and R. Rööm, 2011: High resolution re-analysis for the Baltic Sea region during 1965–2005 period. *Climate Dyn.*, **36**, 727–738, <https://doi.org/10.1007/s00382-010-0842-y>.
- Mahfouf, J., K. Bergaoui, C. Draper, F. Bouyssel, F. Taillefer, and L. Taseva, 2009: A comparison of two offline soil analysis schemes for assimilation of screen level observations. *J. Geophys. Res.*, **114**, D08105, <https://doi.org/10.1029/2008JD011077>.
- Mahmood, S., J. Davie, P. Jermey, R. Renshaw, J. P. George, E. N. Rajagopal, and S. I. Rani, 2018: Indian monsoon data assimilation and analysis regional reanalysis: Configuration and performance. *Atmos. Sci. Lett.*, **19**, e808, <https://doi.org/10.1002/asl.808>.
- Masson, V., 2000: A physically-based scheme for the urban energy budget in atmospheric models. *Bound.-Layer Meteor.*, **94**, 357–397, <https://doi.org/10.1023/A:1002463829265>.
- , and Coauthors, 2013: The SURFEXv7.2 land and ocean surface platform for coupled or offline simulation of earth surface variables and fluxes. *Geosci. Model Dev.*, **6**, 929–960, <https://doi.org/10.5194/gmd-6-929-2013>.
- Mesinger, F., and Coauthors, 2006: North American Regional Reanalysis. *Bull. Amer. Meteor. Soc.*, **87**, 343–360, <https://doi.org/10.1175/BAMS-87-3-343>.
- Mlawer, E. J., S. J. Taubman, P. D. Brown, M. J. Iacono, and S. A. Clough, 1997: Radiative transfer for inhomogeneous atmospheres: RRTM, a validated correlated-*k* model for the longwave. *J. Geophys. Res.*, **102**, 16 663–16 682, <https://doi.org/10.1029/97JD00237>.
- Morcrette, J.-J., 1991: Radiation and cloud radiative properties in the European Centre for Medium-Range Weather Forecasts forecasting system. *J. Geophys. Res.*, **96**, 9121–9132, <https://doi.org/10.1029/89JD01597>.
- Nawri, N., 2014: Evaluation of HARMONIE reanalyses of surface air temperature and wind speed over Iceland. Icelandic Met Office Tech. Rep. 2014–005, 31 pp., [http://www.vedur.is/media/vedurstofan/utgafa/skyrslur/2014/VI\\_2014\\_005.pdf](http://www.vedur.is/media/vedurstofan/utgafa/skyrslur/2014/VI_2014_005.pdf).
- Onogi, K., and Coauthors, 2007: The JRA-25 Reanalysis. *J. Meteor. Soc. Japan*, **85**, 369–432, <https://doi.org/10.2151/jmsj.85.369>.
- Petersen, R. A., 2016: On the impact and benefits of AMDAR observations in operational forecasting. Part I: A review of the impact of automated aircraft wind and temperature reports.

- Bull. Amer. Meteor. Soc.*, **97**, 585–602, <https://doi.org/10.1175/BAMS-D-14-00055.1>.
- Pinty, J.-P., and P. Jabouille, 1998: A mixed-phase cloud parameterization for use in mesoscale non-hydrostatic model: Simulations of a squall line and of orographic precipitation. *Proc. Conf. of Cloud Physics*, Everett, WA, Amer. Meteor. Soc., 217–220.
- Poli, P., and Coauthors, 2013: The data assimilation system and initial performance evaluation of the ECMWF pilot reanalysis of the 20th-century assimilating surface observations only (ERA-20C). ECMWF ERA Report Series, No. 14, 59 pp., <https://www.ecmwf.int/en/elibrary/11699-data-assimilation-system-and-initial-performance-evaluation-ecmwf-pilot-reanalysis>.
- Pottier, P., 2016: Overview of the operational configurations. *Joint ALADIN–HIRLAM Newsletter*, No. 6, Météo-France, Centre National de Recherches Meteorologiques, Toulouse, France, 123–128, <http://www.umr-cnrm.fr/aladin/IMG/pdf/nl6.pdf>.
- Rienecker, M. M., and Coauthors, 2011: MERRA: NASA's Modern-Era Retrospective Analysis for Research and Applications. *J. Climate*, **24**, 3624–3648, <https://doi.org/10.1175/JCLI-D-11-00015.1>.
- Seity, Y., P. Brousseau, S. Malardel, G. Hello, P. Bénard, F. Bouttier, C. Lac, and V. Masson, 2011: The AROME-France convective-scale operational model. *Mon. Wea. Rev.*, **139**, 976–991, <https://doi.org/10.1175/2010MWR3425.1>.
- Simmons, A. J., and D. M. Burridge, 1981: An energy and angular-momentum conserving vertical finite-difference scheme and hybrid vertical coordinates. *Mon. Wea. Rev.*, **109**, 758–766, [https://doi.org/10.1175/1520-0493\(1981\)109<0758:AEAAMC>2.0.CO;2](https://doi.org/10.1175/1520-0493(1981)109<0758:AEAAMC>2.0.CO;2).
- Stepek, A., M. Savenije, H. W. Van den Brink, and I. L. Wijnant, 2015: Validation of KNW atlas with publicly available mast observations (phase 3 of KNW project). KNMI Tech. Rep. 352, 52 pp., <http://publicaties.minienm.nl/documenten/validation-of-knw-atlas-with-publicly-available-mast-observation>.
- Tanré, D., J. Geleyn, and J. Slingo, 1984: First results of the introduction of an advanced aerosol-radiation interaction in the ECMWF low resolution global model. *Aerosols and Their Climatic Effects*, H. Gerber and A. Deepak, Eds., A Deepak Publishing, 133–177.
- Taylor, K. E., R. J. Stouffer, and G. A. Meehl, 2012: An overview of CMIP5 and the experiment design. *Bull. Amer. Meteor. Soc.*, **93**, 485–498, <https://doi.org/10.1175/BAMS-D-11-00094.1>.
- Tegen, I., P. Hollrig, M. Chin, I. Fung, D. Jacob, and J. Penner, 1997: Contribution of different aerosol species to the global aerosol extinction optical thickness: Estimates from model results. *J. Geophys. Res.*, **102**, 23 895–23 915, <https://doi.org/10.1029/97JD01864>.
- Termonia, P., and Coauthors, 2017: The ALADIN system and its canonical model configurations AROME CY41T1 and ALARO CY40T1. *Geosci. Model Dev.*, **11**, 257–281, <https://doi.org/10.5194/gmd-11-257-2018>.
- Toll, V., E. Gleeson, K. Nielsen, A. Männik, J. Mašek, L. Rontu, and P. Post, 2016: Impacts of the direct radiative effect of aerosols in numerical weather prediction over Europe using the ALADIN-HIRLAM NWP system. *Atmos. Res.*, **172–173**, 163–173, <https://doi.org/10.1016/j.atmosres.2016.01.003>.
- Uppala, S. M., and Coauthors, 2005: The ERA-40 re-analysis. *Quart. J. Roy. Meteor. Soc.*, **131**, 2961–3012, <https://dx.doi.org/10.1256/qj.04.176>.
- USGS, 1997: USGS 30 ARC-second Global Elevation Data, GTOPO30. Research Data Archive, Computational and Information Systems Laboratory, National Center for Atmospheric Research, accessed 28 August 2018, <http://rda.ucar.edu/datasets/ds758.0/>.
- Vána, F., P. Bénard, J.-F. Geleyn, A. Simon, and Y. Seity, 2008: Semi-Lagrangian advection scheme with controlled damping: An alternative to nonlinear horizontal diffusion in a numerical weather prediction model. *Quart. J. Roy. Meteor. Soc.*, **134**, 523–537, <https://doi.org/10.1002/qj.220>.
- Whelan, E., J. Hanley, and E. Gleeson, 2017: The MÉRA data archive. Met Éireann Tech. Note 65, 7 pp., <http://hdl.handle.net/2262/81711>.